Fusion Engineering and Design 122 (2017) 204–210

Contents lists available at ScienceDirect

Fusion Engineering and Design

journal homepage: www.elsevier.com/locate/fusengdes

Study on the impacts of pressure equalization slots on MHD flow and safety of FCI in DCLL blanket

Long Chen[a], Shi-Jing Xu[b], Ming-Jian Li[a], Ming-Jiu Ni[a], Nian-Mei Zhang[a,*]

[a] School of Engineering Science, University of Chinese Academy of Sciences, Beijing, China
[b] PetroChina Research Institute of Petroleum Exploration & Development, Beijing, China

ARTICLE INFO

Keywords:
DCLL blanket
FCI
MHD effect
Fluid–structure interaction
Thermal stress

ABSTRACT

For a Dual Coolant Lead Lithium (DCLL) blanket, in order to reduce the pressure difference between inner and outer area of flow channel insert (FCI), which accounts for the stresses in FCI, the pressure equalization slots (PES) are proposed. In the present work, we aim at performing a direct simulation of the magneto-thermal-fluid–structure multi-physical fields in the DCLL blanket, with PES or not, by a coupled computing platform including CFD and the finite element method (FEM), to study the pressure field, velocity field, temperature field and deformation and stresses of FCI. A consistent and conservative scheme and PISO method on an unstructured collocated mesh are employed to solve the incompressible Navier–Stokes equations with the Lorentz force included. The FEM is applied to investigate the thermal strains and stresses of FCI structure. The results show that: (1) inserting FCI with low electrical conductivity and low thermal conductivity, the MHD pressure drop can be reduced and the heat transfer efficiency can be improved; (2) PES does not contribute significantly to pressure equalization. In addition, for case with PES, some potential structural failures and other problems would be caused, such as stress concentration; (3) for the case with PES, although the exit temperature of liquid metal is decreased, the heat transfer efficiency is increased and the max temperature of the first wall (FW) and the temperature difference across FCI wall are decreased.

1. Introduction

The DCLL blanket is a promising concept in the fusion reactor design. In this model, the PbLi circulates for power conversion and tritium breeding; the first wall and blanket structure are cooled by helium (He) [1–3]. With the purpose of reducing the magnetohydrodynamic(MHD) pressure drop, decreasing heat losses and protecting the FW from interacting with the high temperature PbLi, the flow channel insert made of SiC_f/SiC is designed to use inside the channel and manifold, because of its low electrical conductivity and low thermal conductivity [4].

Researchers have been focusing on the MHD and thermal issues of FCI in blanket for decades, such as velocity distribution, the temperature field, the MHD pressure drop and heat transfer [5–7]. Smolentsev et al. [8,9] studied the velocity profiles of MHD flow in the front poloidal. However, the simulation was based on a 2D model for a fully developed flow. Later, Ni et al. [10,11] verified that the liquid metal flow in rectangular duct with FCI was fully 3D flow. And Sutevski et al. [12] conducted a 3D simulation to analyze the effects of PES, as well as two pressure equalization mechanism. They implied that pressure equalization(PE) via electric currents appears to dominate compared to purely hydrodynamic PE. 3D heat transfer simulations based on a static flow field were performed to study the thermal issues by Smolentsev et al. [13,14], without considering the thermal deformation and thermal stresses.

In fact, the DCLL blanket endures affection from both external strong magnetic field and large gradient neutron flux. The liquid metal, FCI structure, magnetic field and heat source constitute a coupling physical field. The high neutron flux formula from neutron analysis [15] demonstrates the relation between space location and heat magnitude. It implies that geometrical configuration of blanket would cause the variation of not only liquid metal flow but also heat transfer. The velocity field, temperature distribution and thermal mechanical behaviors of FCI would change accordingly. In this work, MHD flow, heat transfer and thermal deformation of FCI are investigated by applying 3D CFD simulating code and FE (finite element) method.

2. Description of physical model

The configuration of simplified DCLL blanket channel model with FCI is illustrated in Fig. 1. In the cross-sectional view, the outer steel

* Corresponding author.
E-mail address: nmzhang@ucas.ac.cn (N.-M. Zhang).

http://dx.doi.org/10.1016/j.fusengdes.2017.08.016
Received 1 November 2016; Received in revised form 8 July 2017; Accepted 22 August 2017
Available online 15 September 2017
0920-3796/

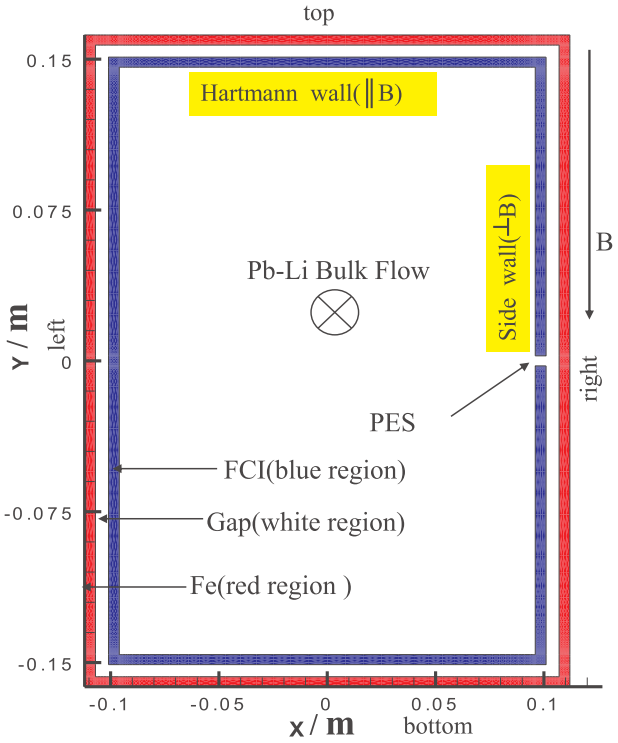

Fig. 1. Cross-section of a poloidal duct with silicon carbide (SiC) flow channel insert (FCI).

wall is cooled by He. The FCI is separated from the ferritic wall by a thin gap filled with liquid metal. These gaps can prevent strong mechanical interaction between the FCI and the ferritic wall with lower temperature. In the following parts, flow inside the FCI is called “bulk flow”, and flow between FCI and ferritic wall is called “gap flow”. In addition, “gap flow” can be distinguished as “Hartmann gap” flow which is perpendicular to the magnetic field, and “Side gap” which is parallel to the magnetic field. The definition of the position “top”, “bottom”, “left” and “right” is shown in Fig. 1 as well. In order to equalize the pressure in these two fluid domains, a PES is set in the FCI wall, as shown in Fig. 1. For convenience, the case without PES is called A; the case with PES in Hartmann wall is called B; the case with PES in Side wall is called C.

In our simulation, liquid metal flows along the poloidal direction (z-direction) with the length of the channel from $z = 0$ to 2000 mm. A uniform strong magnetic field $B_0 = 4$ T is applied paralleling to toroidal direction (y-direction), as shown in Fig. 1. The inlet velocity $\boldsymbol{u}_0$ and the inlet temperature for bulk flow and gap flow is 0.06 m/s and 460 °C, respectively. The radial direction is set along x-direction. The electrical conductivity and thermal conductivity of FCI are $\sigma = 20\ (\Omega\mathrm{m})^{-1}$ and $K = 8$ W/mK, respectively. The other geometrical parameters of the model are provided in Table 1.

Table 1
Geometrical parameters for the Front Poloidal Channel of the reference DCLL blanket.

Regions	Size
Bulk flow (2b × 2a)	192 (mm) × 292 (mm)
FCI thickness	5 mm
Gap thickness	6 mm
Fe thickness	5 mm
PES length	1600 mm
PES width	5 mm

3. Formulation

Actually, the blanket flows are relatively complex, including several feasibility issues. Firstly, the motion of liquid metal, subjected to a strong external magnetic field, induces electrical current, which in turn interacts with the magnetic field and results in a Lorentz force. Compared with the inertial and viscous forces, the Lorentz force is so strong that dominates the flow, determines the velocity distribution and creates a strong MHD pressure drop. Secondly, the heat source produced by neutron reaction, about 10 MW/m^3, will cause the deformation and stresses of the structure, which have a profound impact on the blanket performance, operation and safety. Therefore, the simulation of the magneto-thermal-fluid–structure multi-physical fields appears difficult but significant in order to provide valuable knowledge for liquid-metal blanket design.

3.1. Governing equations for MHD flow

The material properties of the fluid, like its mass density ρ, kinematic viscosity ν, electrical conductivity σ, thermal conductivity K and specific heat capacity C_p are assumed to be constant in the simulation. An external homogeneous magnetic field of amplitude B_0 is applied along the toroidal direction. For most cases of liquid metal flow encountered in industrial applications, the magnetic Reynolds number is very small, so as to the induced magnetic field can be negligible when compared to the imposed magnetic field. Hence, in the present work, it is also assumed that $Rm = \mu\sigma UL \ll 1$, where μ, U and L stand for the fluid magnetic permeability, typical velocity and length scale of the flow respectively, therefore the quasi-static approximation is invoked [16]. Under these assumptions, the magnetohydrodynamic equations governing the flow can be written as

$$\nabla\cdot\vec{\mathbf{u}} = 0 \tag{1}$$

$$\frac{\partial\vec{\mathbf{u}}}{\partial t} + (\vec{\mathbf{u}}\cdot)\vec{\mathbf{u}} = -\frac{1}{\rho}\nabla p + \frac{1}{\rho}(\vec{\mathbf{j}} \times \vec{\mathbf{B}}) + \nu\Delta\vec{\mathbf{u}} \tag{2}$$

$$\vec{\mathbf{j}} = \sigma(-\nabla\Phi + \vec{\mathbf{u}} \times \vec{\mathbf{B}}) \tag{3}$$

$$\nabla\cdot\vec{\mathbf{j}} = 0 \tag{4}$$

$$\rho C_p\left(\frac{\partial T}{\partial t} + \vec{\mathbf{u}}\cdot\nabla T\right) = \nabla\cdot(K\nabla T) + \frac{\vec{\mathbf{j}}^2}{\sigma} + Q \tag{5}$$

where the variables $\vec{\mathbf{j}}$, Φ, $\vec{\mathbf{u}}$, denote current density, electric potential and velocity, respectively. And Q is the thermal load deposited by the high neutron flux [15], $Q = 3 \times 10^7 e^{-10(x+b)}$, where b is half length of bulk flow along x direction.

The different cases that we will consider can be characterized by two non-dimensional numbers. One is the Reynolds number, $Re = UL/\nu$, representing the ratio of inertial to viscous forces. The other is the Hartmann number, $\mathrm{Ha} = \mathrm{LB}_0\sqrt{\sigma/\rho\nu}$, which characterizes the ratio of electromagnetic to viscous forces. In addition, the interaction parameter, which can be expressed in terms of Hartmann number and Reynolds number, $N = \mathrm{Ha}^2/\mathrm{Re} = \sigma\mathrm{LB}_0^2/\rho U$, standing for the ratio of electromagnetic to inertial forces, appears important as well. According to the Hartmann–Reynolds relationship [17], the present blanket flows, Ha = 13,089 and Re = 47,872, are expected to be quasi-two-dimension (Q2D) turbulent.

In the build-up of the present numerical code, PISO [18] algorithm is introduced to treat the pressure–velocity coupling equations including the Lorentz force term in fluid field. The finite volume method is employed to discrete the incompressible Navier–Stokes equations, electrodynamics equations and energy equation in the node-based formulation. The PISO loop consists of an implicit momentum predictor followed by a series of pressure solutions and explicit velocity corrections. The loop is repeated until a pre-determined tolerance is reached.

During the loop, the Lorentz force term is treated explicitly as an additional force term.

With regard to the simulation of MHD flow, especially for high Hartmann number, the calculation of Lorentz force appears very challenging. Therefore, at present study, the electric Poisson equation is solved according to the consistent and conservative scheme developed by Ni et al. [19,20].

3.2. Governing equations for solid structure

Geometric equation for small deformation in FCI considering thermal effect is

$$\varepsilon_{ij} = \frac{1}{2}(d_{i,j} + d_{j,i}) + \alpha \Delta T \delta_{ij} \tag{6}$$

where ε_{ij} represents strain tensor. d_i represents displacement vector. ΔT describes the temperature variation of solid structure. α is thermal expansion coefficient. δ_{ij} is the Kronecker delta.

$$\delta_{ij} = 1(i = j)$$
$$\delta_{ij} = 0(i \neq j) \tag{7}$$

As described by Abdou et al. [21], SiC is the candidate material for FCI because of its good electrical and thermal insulating characteristic. And its constitutive relation meets generalized Hooke law in elastic state. Considering the small deformation of FCI structure, the constitutive equation would describe the linear relation between strains and stresses.

$$\sigma_{ij} = 2G\varepsilon_{ij} + \lambda \Theta \delta_{ij} \tag{8}$$

Here, σ_{ij} is defined as stress tensor. G is shear modulus and $\lambda = E\mu/[(1 + \mu)(1 - \mu)]$ is Lame constant. $\Theta = \varepsilon_{ii}$ is volumetric strain and μ is Poisson's ratio. And the equilibrium equations of structure satisfy

$$\sigma_{ij,j} + F_i = 0 \tag{9}$$

where F_i is the ith component of volumetric force.

3.3. Boundary conditions

Boundary conditions are given at inlet by specifying a uniform or fully developed velocity profile. A no-slip boundary condition is applied on the other walls, $\vec{\mathbf{u}}_{wall} = 0$. At the outlet, the fully developed condition is imposed:

$$U_x = U_y = \frac{\partial U_z}{\partial n} = 0 \tag{10}$$

Hereinafter $\vec{\mathbf{n}}$ denotes the unit normal to the boundaries, including all the rigid walls, inlet and outlet of liquid metal.

Insulating conditions, $\vec{\mathbf{j}} \cdot \vec{\mathbf{n}} = 0$, are adopted for the electrical current density $\vec{\mathbf{j}}$ at all the boundaries. Therefore, Neumann condition is specified for electrical potential at the insulated walls $\partial\phi/\partial n = 0$, except the inlet and outlet of liquid metal, where the following boundary condition is used:

$$\frac{\partial \phi}{\partial n} = (\vec{\mathbf{u}} \times \vec{\mathbf{B}}_0) \cdot \vec{\mathbf{n}} \tag{11}$$

With regard to the temperature boundary of liquid metal, a fixed value is given at the inlet and $\partial T/\partial n = 0$ is specified at the outlet. For FCI and FW, insulating condition $\partial T/\partial n = 0$ is adopted at $z = 0$ and $z = 2000$ mm, while the outside walls of the FW is set to satisfy convective boundary condition,

$$K\frac{\partial T}{\partial n} + h(T - T_{ref}) = 0 \tag{12}$$

where h is convective heat transfer coefficient, for helium $h = 4000$ W/m^2 K. The temperature in the helium flows, T_{ref}, is fixed at 400 °C.

For the interfaces between gap flow and FCI, or bulk flow and FCI, solutions are coupled by ensuring the continuity of wall temperature $T_f = T_s$, heat flux $q_f'' = q_s''$, wall electric potential $\phi_f = \phi_s$ and wall normal current $j_{n,f} = j_{n,s}$. Here, the subscript f and s represent the fluid side and structure side of the interface, n means the unit normal of the interface.

3.4. Steady fluid–structure interaction

The study focused on the magneto-thermal-fluid–structure multi-physical fields has been done by many researchers, such as Smolentsev et al. [13,14]. However, only in the process of solving temperature field, three dimensional simulations were conducted, which covered the effect of the strong heat source. To the best of our knowledge, no published simulations on the multi-physical fields concern the fluid–-structure interaction, including solving deformation and stresses in FCI. Thus, one of the main objectives for this study is to investigate the influence of temperature fields, resulting from our CFD calculation directly, on deformation and stresses in FCI (with PES). At present, a steady fluid–structure interaction is under consideration. In other words, the influence of deformation of FCI on the flow fields is neglected, which will be involved in our next study plan.

In addition, sequential method, which is widely used to simulate the fluid–structure interaction, is employed to investigate temperature distribution and thermal deformation of FCI in the magneto-thermal-fluid–structure coupled field. Fig. 2 indicates the calculating process of steady fluid–structure interaction (FSI). Initially, conjugate heat transfer in both fluid and structure are analyzed. Then the surface temperature of FCI is transmitted to structure as boundary conditions. Finally, finite element analysis method is employed to solve deformations and stresses in FCI.

4. Results and analysis

4.1. MHD effects

In the liquid metal blanket, MHD pressure drop is always a key issue for research, because it is related to the pumping capacity of rotary pumps directly. Therefore, a group of numerical simulations were conducted to study the MHD pressure drop in DCLL blanket. According to the numerical results of Smolentsev et al. [13,14], FCI plays a key role in the reduction of pressure drop. The pressure drop reduction factor $R = ((dp/dx)_0/(dp/dx))$, can reach about 120 for FCI with low electrical conductivity, $\sigma = 20\ (\Omega m)^{-1}$. Here $(dp/dx)_0$ and (dp/dx) represent pressure gradient without FCI and pressure gradient with FCI, respectively, However, the calculation results from the fully developed flow, simulated by a two dimensional model, which has been proved not real case [10–12]. But the model both of them used is from a FCI experimental apparatus with GaInSn, which conducted at Southwestern Institute of Physics. Thus, according to the real size of the Front Poloidal Channel of DCLL blanket, we perform a three dimensional simulation to do a MHD thermohydraulics analysis.

As shown in Fig. 3, the MHD pressure drop can be reduced by inserting FCI with low electrical conductivity. For the liquid metal flow with uniform inlet velocity, it can be noted that the pressure distribution can be divided into two parts, developing flows region and fully developed flows region. In the developing flows region, which length is 4–5 times of the width of the flow channel downstream inlet, high pressure drop still exists ($\Delta p \sim 2.4 \times 10^{-2}$ MPa). However, for the fully developed flows, the pressure gradient keeps constant and the pressure drop reduces to $\Delta p \sim 10^{-3}$ MPa. This is because, in fully

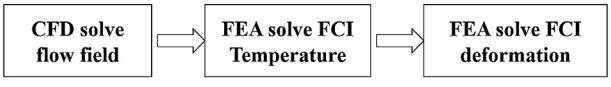

Fig. 2. The working process of steady state FSI.

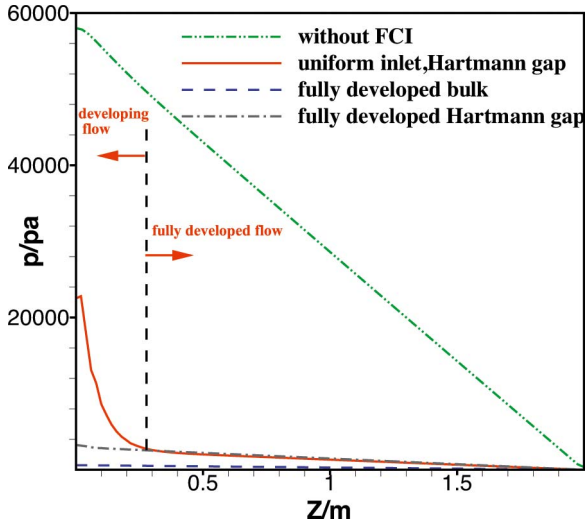

Fig. 3. Comparison of pressure distribution.

developed flows region, the opposing Lorentz forces arise from the interaction between the induced cross-sectional currents closing in the toroidal-radial plane and the strong toroidal magnetic field. With a high interaction number N, we have $\Delta p \approx \vec{j} \times \vec{B}$. So when an almost insulated FCI is introduced, current density is reduced significantly compared to the case without FCI. Moreover, when a fully developed velocity is applied at inlet, the pressure drop is reduced from $\Delta p \sim 6 \times 10^{-2}$ MPa to $\Delta p \sim 4 \times 10^{-3}$ MPa and the pressure drop reduction factor R can reach about 112. But the flow is still three dimensional, which can be characterised by the different pressure gradient of gap flow and bulk flow.

As the FCI is introduced, pressure field changes a lot. Not only the pressure drop decreases which has been mentioned above, but also a non-uniform pressure distribution in a cross-section occurs, which implies that flow with FCI is a typical 3D flows, as shown in Fig. 4. These results agree with the conclusions, “3D pressure drop”, obtained by Ni et al. [10,11] and Sutevski et al. [12]. Moreover, near the inlet, pressure difference is huge not only between bulk flow and gap flow but also between the different positions of gap flow. It is interesting to note that the pressure drop of bottom gap and top gap is larger than any other locations. All of these differences are related with the distribution of the electrical current. For instance, in the Hartmann gap near inlet, a strong current density circulates in a thin area, compared with side gap, thus large pressure drop occurs.

It is precisely because of the existence of pressure difference between bulk flow and gap flow, PES in FCI wall is introduced. However, the balancing effect for both case B and case C is not promising. As shown in Fig. 4(b) PES opened in Hartmann wall can effectively balance the pressure difference between gap flow and bulk flow near the slot. The lines stand for pressure distribution along the center of top gap and center of bulk flow are coincidence for fully developed flow, which demonstrates the effect. However, for other positions, the pressure differences are still huge. PES placed in the Side wall, as shown in Fig. 4(c), can not balance the pressure difference at all. In addition, our numerical results reveal that the stress of FCI caused by the pressure difference is much less than that caused by the thermal load. In this respect, the design of PES appears meaningless as well.

When FCI with low electrical conductivity is inserted into the blanket, the electrical currents stream lines from bulk flow to gap flow are cut off. Therefore, for the almost insulated FCI, the bulk flow fully matches the Shercliff flow. And in the Hartmann gaps, the flow is almost stagnant. However, in each side gap, a jet flow can be found, as shown in Fig. 5(a). With PES in Hartmann wall, a weak velocity jump is formed around PES, as shown in Fig. 5(b). Because the current density in the PES is slightly stronger than the other position inside FCI, which means a stronger x component of current density j_x and a stronger Lorentz force. Moreover, as shown in Fig. 5(d), velocity near the left side wall for case B is larger than that of case A. When PES is placed in the side wall, a strong reversed velocity appears in the PES, shown in Fig. 5(c). Because a very strong x component of current density j_x formed there introduces a strong opposing Lorentz force. Moreover, the velocity near the left side wall for case C is the largest. The velocity distribution of present study resembles the results of Smolentsev et al. [13].

4.2. Thermal issues

In this section, the thermal issues, including temperature fields and thermal deformation and thermal stress will be discussed.

As thermal insulator, one of the advantages of FCI is that it can improve the exit temperature of liquid metal. The typical temperature distributions at the outlet is illustrated in Fig. 6, which agree with the results of Smolentsev et al. [13,14]. As shown in the figure, for the bulk flow, temperature field varies intensely in the radial direction while changes gently in the toroidal direction. However, in both radial and toroidal direction, the changes in temperature field are large near the inside ferritic steel wall cooled by the helium flows. Due to the heat transfer effect by the liquid metal, temperature field reaches the peak value at the exit.

From the respect of “pressure difference”, we have concluded that the introduction of PES is not significant. Here, the effect of PES on the temperature distribution is analyzed. Compared with case A, the exit temperatures of PbLi for case B and case C are lower. The first reason is that the energy of bulk flow can be transferred to the outside region, especially for case C. As shown in Fig. 6(c), the complex velocity distribution, jets and reverse velocity, enhance the heat transfer in the radial direction. Secondly, it is related to the velocity distribution near the left side wall where the strongest heat source located. As shown in Fig. 5(d), near the left side wall, the velocity of case C is bigger than that of case B, while case A is the smallest one. These two reasons result in the lower exit temperature distribution, which is a disadvantage of

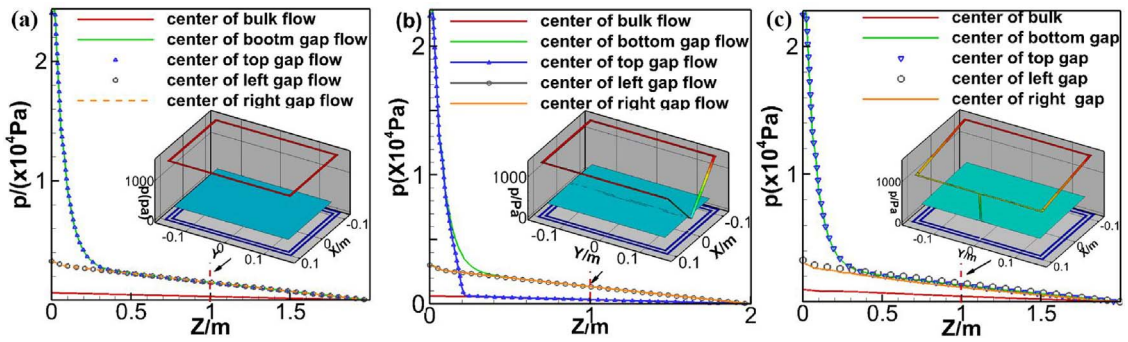

Fig. 4. Pressure distribution along flow direction at different positions and pressure distribution at $z = 1$. (a) Without PES; (b) PES on the Hartmann wall; (c) PES on the side wall.

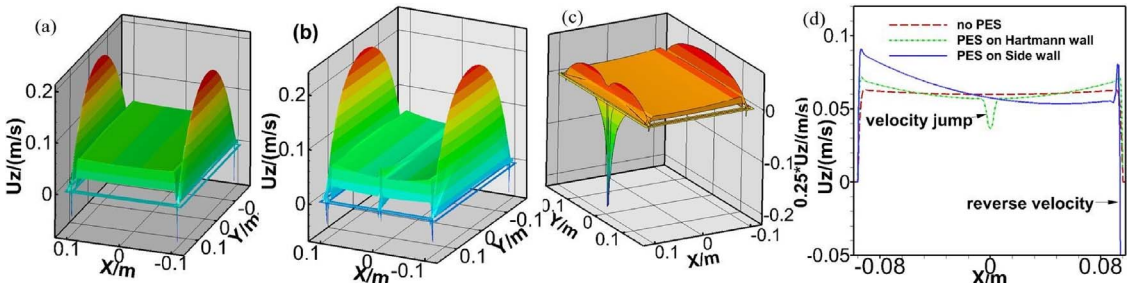

Fig. 5. Velocity distribution at $z=1$. (a) Case A; (b) case B; (c) case C; (d) comparison along z = 1, y = 0.

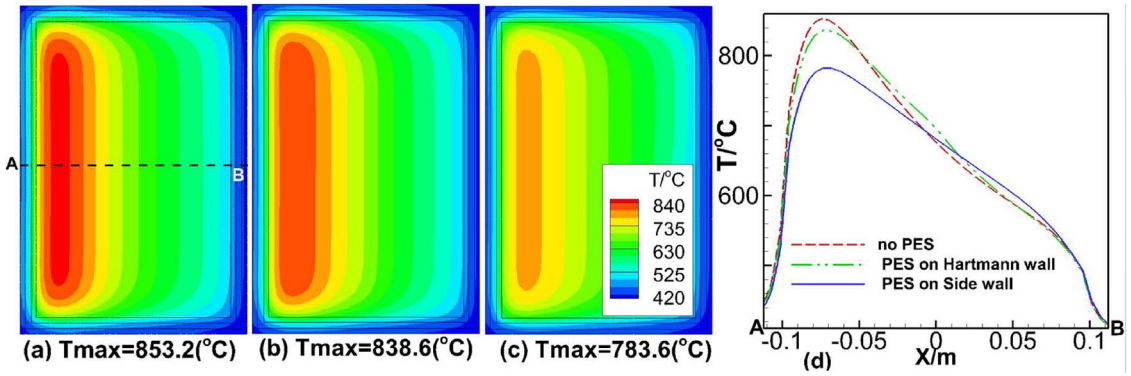

Fig. 6. Temperature distribution of outlet. (a) Case A; (b) case B; (c) case C; (d) comparison along line AB.

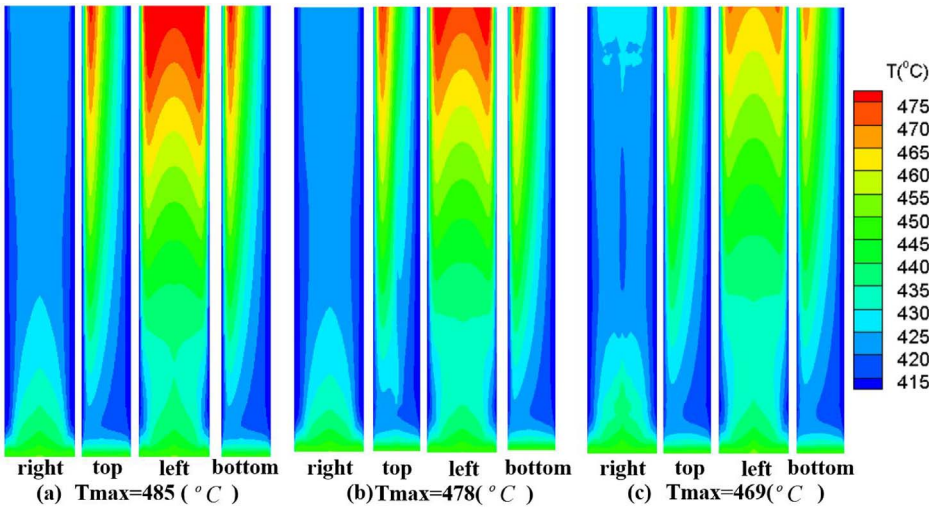

Fig. 7. Temperature distribution of first wall at the interface between gap flow and Fe wall. (a) Case A; (b) case B; (c) case C.

PES.

Based on the allowable corrosion rate, ferritic steel wall temperature is usually limited to 480 °C. Fig. 7 shows the temperature on the inner face of the first wall. The highest temperatures occur at left wall no matter whether a PES is employed. However, with PES in FCI wall, the max temperature of left interface is lower than 480 °C which is an advantage of PES. Similarly, case C is the most safe design. Moreover, it can be found that PES has little influence on the temperature distribution of interface where the slot located.

Considering the thermal deformation and stress, temperature difference across the FCI wall is usually limited to 200 °C. The distribution of temperature difference across FCI is shown in Fig. 8. The max temperature difference appears on the left wall of FCI as well and it is reduced with PES in wall. This is another advantage of PES. The temperature difference through FCI thickness depends on both the heat amount carried away by poloidal flow of metal fluid in both bulk and gap, and heat transfer with the FW cooled by helium coolant. According to the velocity distribution shown in Fig. 5, the temperature differences distribution is easy to be understood especially near the slot.

Fig. 9 indicates stress distributions of FCI with PES in wall. For case B, the maximum stress appears at the edge of Hartmann wall outlet, and it is larger than that of case C (the maximum stress appears near the slot in this case). It is obvious that PES will cause stress concentration near the end of the slot. In addition, when PES is in side wall, this effect will be larger (from Fig. 9(c)). The distribution of stresses is the compound effect caused by temperature, temperature difference through the wall thickness and structural characterization.

5. Conclusions

In this paper, a direct simulation of 3D liquid metal flow in the DCLL blanket under external magnetic field is conducted to study the velocity distribution and temperature field in the blanket. A consistent and conservative scheme and PISO method on an unstructured collocated

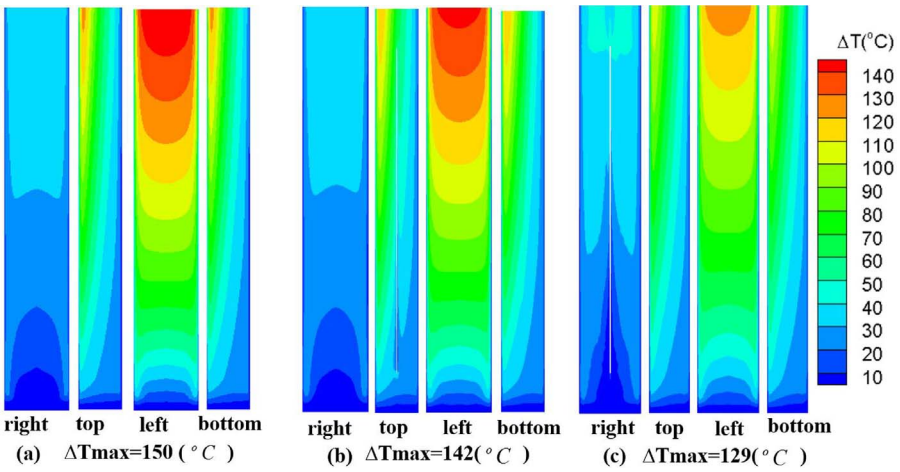

Fig. 8. Temperature difference distribution across FCI. (a) Case A; (b) case B; (c) case C.

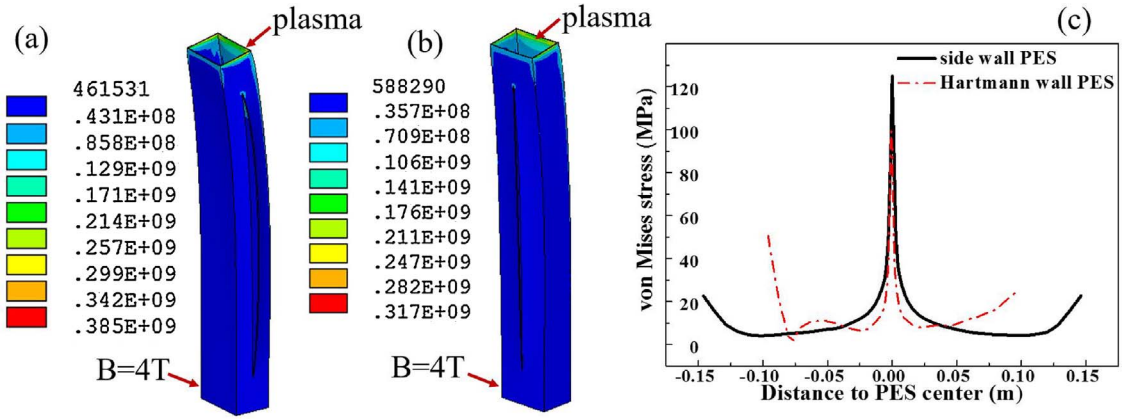

Fig. 9. Mises stress distribution of FCI with PES. (a) Case B; (b) case C; (c) stress concentration near the slot end in wall with PES.

Table 2
Comparison between the four cases.

Case	MHD pressure drop	T_{max} of outlet	T_{max} of first wall	ΔT_{max} across FCI	heat transfer efficiency (η)
Without FCI	0.058 MPa	966.5 T °C	496 T °C		85.2%
Case A	0.0245 MPa	853.2 T °C	485 T °C	150 T °C	87.9%
Case B	0.023 MPa	838.6 T °C	478 T °C	142 T °C	89.2%
Case C	0.023 MPa	738.6 T °C	469 T °C	129 T °C	88.8%

mesh are employed to solve the incompressible Navier–Stokes equations with the Lorentz force included. The FEM is applied to investigate the thermal strains and stresses of FCI structure. The magneto-thermal-fluid–structure coupled fields are simulated. The effects of slots in either side wall or Hartmann wall of FCI are analyzed. The safeties of FCI are evaluated by equivalent stress and peak temperature. Several important results have been summarized as Table 2.

Here the heat transfer efficiency is calculated as $\eta = P_{PbLi}/P_{heat\ source}$, where $P_{PbLi} = \int\int_{out}(\rho C_p U_{out} T_{out})dS - \int\int_{in}(\rho C_p U_{in} T_{in})dS$, $P_{heat\ source} = \int\int\int_V 3 \times 10^7 e^{-10(x+b)} dV$. The results show that:

(1) Inserting FCI with low electrical conductivity and low thermal conductivity, the MHD pressure drop can be reduced and the heat transfer efficiency can be improved effectively.
(2) Only when PES placed in Hartmann wall, the pressure difference can be balanced, while the effect is confined in the vicinity of the slot. PES does not contribute significantly to pressure equalization.
(3) For case with PES, although the exit temperature of liquid metal is decreased, the heat transfer efficiency is increased and the max temperature of the FW and the temperature difference across FCI are decreased.
(4) With PES in FCI wall, some potential structural failures and other problems will be caused, such as stress concentration.

Acknowledgements

The authors gratefully acknowledge the support from the NSFC (Natural Science Foundation of China) under Grants #51376175, #51636009, #51606183 and ITER Programme from Ministry of Science and Technology of China under Grant #2013GB114000.

References

[1] M.A. Abdou, Perspective on fusion energy, Proceedings of TWAS-ARO Meeting, Bibliotheca Alexandrina, 2009, p. 4.
[2] M.S. Tillack, S. Malang, High performance PbLi blanket, Proceedings of the 17th IEEE/NPSS Symposium on Fusion Energy, San Diego, CA, 1997, pp. 1000–1004.
[3] M.A. Abdou, D. Sze, C. Wong, M. Sawan, A. Ying, N.B. Morley, S. Malang, US plans and strategy for ITER blanket testing, Fusion Sci. Technol. 47 (2005) 475–487.
[4] N.B. Morley, Y. Katoh, S. Malang, B.A. Pint, A.R. Raffray, S. Sharaft, S. Smolentsev, G.E. Youngblood, Recent research and development for the dual coolant blanket concept in the US, Fusion Eng. Des. 83 (2008) 920–927.
[5] Z.Y. Xu, C.J. Pan, X.J. Zhang, L. Zhao, J. Zhang, G.J. Yang, Primary experimental results of MHD flow in the duct with flow channel insert, Nucl. Fusion Plasma Phys. 29 (2009) 6–9.
[6] M.A. Abdou, N.B. Morley, A.Y. Ying, S. Smolentsev, P. Calderoni, Overview of fusion blanket R & D in the US over the last decade, Fusion Eng. Technol. 37 (2005) 401–422.
[7] D. Sutevski, S. Smolentsev, N.B. Morley, M.A. Abdou, 3D numerical study of MHD flow in a rectangular duct with flow channel insert, Fusion Sci. Technol. 50 (2006) 107–119.
[8] S. Smolentsev, M.A. Abdou, N.B. Morley, et al., Numerical analysis of MHD flow

and heat transfer in a poloidal channel of the DCLL blanket with a SiC_f/SiC flow channel insert, Fusion Eng. Des. 81 (2006) 549–553.
[9] S. Smolentsev, N.B. Morley, M.A. Abdou, Code development for analysis of MHD pressure drop reduction in a liquid metal blanket using insulation technique based on a fully developed flow model, Fusion Eng. Des. 73 (2005) 83–93.
[10] M.J. Ni, S.J. Xu, Z.H. Wang, N.M. Zhang, Direct simulation of three-dimensional MHD flows in liquid metal blanket with flow channel insert, Fusion Sci. Technol. 60 (2011) 292–297.
[11] S.J. Xu, M.J. Ni, Direct simulation of MHD flows in dual-coolant liquid metal fusion blanket using a consistent and conservative scheme, Theo. Appl. Mech. Lett. 1 (2011) 1–4.
[12] D. Sutevski, S. Smolentsev, M.A. Abdou, 3D numerical study of pressure equalization in MHD flow in a rectangular duct with insulating flow channel insert, Fusion Sci. Technol. 89 (2014) 1370–1374.
[13] S. Smolentsev, N.B. Morley, M.A. Abdou, Magnetohydrodynamic and thermal issues of the SiC_f/SiC flow channel insert, Fusion Sci. Technol. 50 (2006) 107–119.
[14] S. Smolentsev, N.B. Morley, C. Wong, M.A. Abdou, MHD and heat transfer considerations for the US DCLL blanket for DEMO and ITER TBM, Fusion Eng. Des. 83 (2008) 1788–1791.
[15] R.E. Alcouffe, R.S. Baker, F.W. Brinkley, DANTSYS 3.0: A Diffusion Accelerated Neutral Particle Transport Code System, LA-12969-M, Los Alamos National Laboratory, 1995.
[16] U. Schumann, Numerical simulation of the transition from three to two-dimensional turbulence under a uniform magnetic field, J. Fluid Mech. 74 (1976) 31–58.
[17] S. Smolentsev, S. Badia, R. Bhattacharyay, et al., An approach to verification and validation of MHD codes for fusion applications, Fusion Eng. Des. 100 (2015) 65–72.
[18] R. Issa, Solution of the implicitly discretized fluid flow equation by operator splitting, J. Comp. Phys. 62 (1986) 40–65.
[19] M.J. Ni, R. Munipalli, N.B. Morley, et al., A current density conservative scheme for incompressible MHD flows at a low magnetic Reynolds number. Part I: On a rectangular collocated grid system, J. Comp. Phys. 227 (2007) 174–204.
[20] M.J. Ni, R. Munipalli, P. Huang, et al., A current density conservative scheme for incompressible MHD flows at a low magnetic Reynolds number. Part II: On an arbitrary collocated mesh, J. Comp. Phys. 227 (2007) 205–228.
[21] C.P.C. Wong, M.A. Abdou, M. Dagher, et al., An overview of the US DCLL ITER-TBM program, Fusion Eng. Des. 85 (2010) 1129–1132.